Interference Analysis for Millimeter-Wave Networks With Geometry-Dependent First-Order Reflections

Miaomiao Dong and Taejoon Kim, *Member, IEEE*

***Abstract*—Recent experimental studies reveal that urban millimeter wave (mmWave) channels are often dominated by both the line-of-sight (LoS) and geometry-dependent first-order reflection paths. In such environments, it is possible that any LoS and/or reflection components from surrounding interferers can critically deteriorate the link quality. Analyzing such impacts is, however, challenging in the absence of appropriate mmWave network interference models. In this correspondence paper, we address this challenge by providing an analytical stochastic geometry model that quantifies the total amount of network interference. Our study reveals that dense mmWave networks are often interference limited. The geometry-dependent first-order reflection interference is a dispensable component and must be encountered when analyzing and designing mmWave networks.**

***Index Terms*—First-order reflection, interference analysis, millimeter wave networks, stochastic geometry.**

I. Introduction

In millimeter wave (mmWave) bands, the radio channel experiences severe pathloss which is compensated for by using highly directional narrow beams. These directional beams can be blocked or reflected by obstacles. Interference occurs when the signals emitted from surrounding unintended transmitters are captured by the beam at an intended receiver via line-of-sight (LoS) and/or reflection paths. This interference event can be of a small probability. However, when it comes with a large number of unintended transmitters, their accumulated effect can critically exacerbate the link quality.

The Poisson point process (PPP) in stochastic geometry has been widely employed to accurately model the distributions of urban mmWave base stations and obstacles [1]–[4]. The work in [1] characterized the mmWave link outage due to the LoS interference. Exploiting the PPP, the mean power [2], complementary cumulative distribution function (CCDF) [3], and signal-to-interference ratio [4] of mmWave LoS interference links have been characterized. The work in [1]–[4], however, does not consider the existence of first-order reflection interference. Recently, there have been convincing measurement results showing that urban mmWave links are often dominated by both the LoS and first-order reflection paths [5].

Manuscript received October 16, 2017; revised March 18, 2018, July 5, 2018, and August 24, 2018; accepted October 8, 2018. Date of publication October 17, 2018; date of current version December 14, 2018. The work of T. Kim was supported by The University of Kansas under Start-Up Fund. The review of this paper was coordinated by Dr. L. Dai. *(Corresponding author: Miaomiao Dong.)*

M. Dong is with the Department of Electronic Engineering, City University of Hong Kong, Kowloon Tong, Hong Kong (e-mail: mmdong2-c@my.cityu.edu.hk).

T. Kim is with the Department of Electrical Engineering and Computer Science, The University of Kansas, Lawrence, KS 66045 USA (e-mail: taejoonkim@ku.edu).

Color versions of one or more of the figures in this paper are available online at http://ieeexplore.ieee.org.

Digital Object Identifier 10.1109/TVT.2018.2876501

In mmWave links, the first-order reflection paths are geometry-dependent [5], [6]. This dependency, however, makes the interference analysis challenging due to the complicated reflection and blockage mechanism. Recently, the statistics of geometry-dependent first-order reflection paths of a point-to-point (P2P) mmWave link were analyzed [6], where the random obstacles are assumed to have a common rotation angle. The P2P model in [6], however, cannot be directly extended to a network model. In practical networks, the obstacles can have random orientations. Conventional view has been pessimistic about analyzing the accumulated effect of the random LoS and geometry-dependent reflection interference.

In this paper, we provide an analytical LoS and reflection interference model and statistically quantify the accumulated effect of them in a dense urban mmWave network. We assume the obstacles and transmitters are distributed according to PPP. The obstacles have independent and identically distributed (i.i.d.) rotation angles and sizes. The distributed unintended transmitters can generate interference through either the LoS or first-order reflection paths. Under these assumptions, we find the mean and CDF of the accumulated network interference power. Our results signify that dense urban mmWave networks are often interference-limited. The reflection interference power is less than the LoS interference, but is far above the noise level. Hence, when designing and analyzing mmWave networks, the effect of the geometry-dependent reflection interference, which was often ignored, must be taken into account.

II. Network Setup

In this section, the network model under consideration and the assumptions made in subsequent derivations are provided. The key notations frequently used throughout the paper are given as below: $\overline{\mathrm{AB}}$ is the line segment connecting points A and B, $L_{\overline{\mathrm{AB}}}$ is the length of $\overline{\mathrm{AB}}$, $\Pr_{\mathcal{A}}(x)$ is the probability of random event $\mathcal{A}$ which is a function of x, $E_N(x)$ is the expectation of N which is a function of x, and $\mathbf{O}(r)$ is the circle centered at $(0,0)$ with radius r.

A. Network Model

Consider an urban mmWave network, which consists of multiple transmitters, receivers, and obstacles. Each transmitter (receiver) employs a directional narrow beam. The obstacles in the network can block or reflect the narrow beams. Each receiver is associated with its nearest visible LoS transmitter that meets the link budget condition and regards other unintended transmitters as potential interferers[1]. As shown in Fig. 1, we focus on the receiver placed at $(0,0)$ in $\mathbb{R}^2$. Between the considered receiver and an unintended transmitter, there may exist an LoS or reflection path. In the case when both the beams of the considered receiver and unintended transmitter are aligned with this LoS or reflection path, interference will be imposed. As shown in Fig. 1, the reflection paths are generated by obstacles, obeying the

[1]It may exist visible reflection paths whose lengths are smaller than the nearest visible LoS distance. Because the power along a reflection path is much weaker than that of an LoS path, we consider, in this work, LoS association only.

0018-9545 © 2018 IEEE. Personal use is permitted, but republication/redistribution requires IEEE permission.
See http://www.ieee.org/publications_standards/publications/rights/index.html for more information.

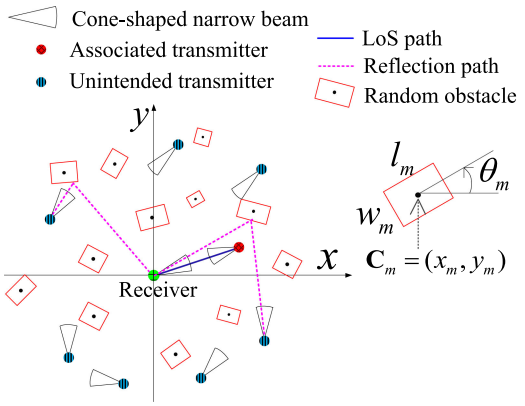

Fig. 1. Urban mmWave network.

specular reflection theory (i.e., the angle of incident is equal to the angle of reflection). The length of a first-order reflection path is the sum length of the two line segments constituting the reflection path.

B. Assumptions

Assumption 1: An obstacle m is rectangular-shaped and is defined by a quadruple $\{\mathbf{C}_m = (x_m, y_m), l_m, w_m, \theta_m\}$, where the $\mathbf{C}_m$, l_m, w_m, and θ_m denote, respectively, the center coordinates, length, width, and rotation angle of obstacle m, as shown in Fig. 1. Here, the θ_m measures the anti-clockwise rotation angle from the positive x-axis to the l-side of obstacle m. The set $\{\mathbf{C}_m\}$ obeys a homogeneous PPP on $\mathbb{R}^2$ with density λ_{Obs}. We assume l_m, w_m, and θ_m are mutually independent. The random variables $\{l_m\}$ (respectively, $\{w_m\}$ and $\{\theta_m\}$) are i.i.d. according to a uniform distribution in the interval $l_m \in [l_{Min}, l_{Max}]$ (resp., $w_m \in [w_{Min}, w_{Max}]$ and $\theta_m \in [0, \pi)$).

Assumption 2: We set the maximum link distance as $R_{Max} =$ 200 m, which is measured at the 28 GHz band in an urban scenario with the transmit power $P_{TX} = 30$ dBm [7][2]. The received signal strengths along the paths with their lengths larger than R_{Max} become weak and negligible. Therefore, we discard any path with the length larger than R_{Max}.

Assumption 3: Since the sizes of transmitters are much smaller than obstacles, the transmitters do not block any links. We assume the distribution of transmitters obeys a homogeneous PPP on $\mathbb{R}^2$ with density λ_{TX}. The distance $d \in (0, R_{Max}]$ between the considered receiver and its associated transmitter is then a random variable that follows the probability density function (PDF) [4, Corollary 8.1]

$$f_d(x) = 2\pi x \lambda_{TX} \exp\left(-\beta x - p - 2\pi\lambda_{TX} U(x)\right), \quad (1)$$

where $p = \lambda_{Obs} E_l E_w$, $\beta = 2\lambda_{Obs}(E_l + E_w)/\pi$, and $U(x) = e^{-p}[1 - (\beta x + 1)e^{-\beta x}]/\beta^2$.

Assumption 4: For a tractable analysis, we assume the directional beams at the transmitters and receiver in Fig. 1 obey the cone-shaped beam pattern defined by

$$G(\phi) = \begin{cases} \frac{2\pi}{\Delta}, & \text{if } -\frac{\Delta}{2} \le \phi \le \frac{\Delta}{2} \\ 0, & \text{otherwise} \end{cases}, \quad (2)$$

[2]The 28 GHz is one of the standardized bands for the 5G cellular operation [7], while the 30 dBm is a typical transmit power value of 3GPP micro-cell base stations [4], [7].

where $G(\phi)$ is the array gain with boresight direction ϕ uniformly distributed in $[0, 2\pi)$ and Δ is the mainlobe beamwidth in radian. The transmitters and the receiver have different beamwidths, denoted by Δ_{TX} and Δ_{RX}, respectively. The probability that the beams of an unintended transmitter and the receiver are aligned along a path is then given by $\frac{\Delta_{TX}\Delta_{RX}}{4\pi^2}$.

Assumption 5: We admit the LoS pathloss model at 28 GHz in [8], i.e., $PL_{LoS}(r) = 61.4 + 20\log 10(r)$ in dB, where r is the LoS path length in meter. For a first-order reflection path with length r, we use the pathloss model in [9], i.e., $PL_{Ref}(r) = 61.4 + 20\log 10(r) + RL$ in dB, where RL is the reflection loss. Once a $q \in \{LoS, Ref\}$ path of length r presents with which both the beams of the considered receiver and an unintended transmitter are aligned, the interference power is given by

$$I_q(r) = P_{TX} G_{TX} G_{RX} 10^{-\frac{PL_q(r)}{10}}, \quad (3)$$

where G_{TX} and G_{RX} are, respectively, the transmit and receiver array gains and follow (2), e.g., $G_{TX} = \frac{2\pi}{\Delta_{TX}}$.

III. Preliminaries

In this section, we summarize two existing stochastic models for a P2P mmWave link, and based on these, derive useful statistics that will be used in the sequel. We focus on the P2P link from the unintended transmitter at $(D, 0)$ to the receiver at $(0, 0)$ in Fig. 2. For ease of description, we denote the unintended transmitter as T and the intended receiver as R.

A. First-Order Reflection: Ellipse Model

The *Ellipse Model* in [6] can be exploited to characterize the average number of reflection paths of a P2P link. The *Ellipse Model* is based on the fact that the reflection points of all the first-order reflection paths with the same length $r \in (D, D_{Max}]$ reside on a common ellipse, defined by

$$\Omega(r) = \left\{(x, y) : \frac{(x - D/2)^2}{r^2/4} + \frac{y^2}{(r^2 - D^2)/4} = 1\right\}, \quad (4)$$

where the foci of $\Omega(r)$ are the T and R, as shown in Fig. 2(a).

For obstacles with an arbitrary rotation angle θ, there are four possible reflection points Z_1, Z_2, Z_3, and Z_4 on the ellipse $\Omega(r)$, shown in Fig. 2(a). The coordinates of $\mathrm{Z}_i = \left(x_{\mathrm{Z}_i}(\theta, r, D), y_{\mathrm{Z}_i}(\theta, r, D)\right)$, $i \in \{1, 2, 3, 4\}$ can be computed by using [6, (12) and (13)]. The first-order reflection path at Z_i exists if and only if the following two events occur: (i) Event $\mathcal{A}_i$: The reflection path is created at Z_i by the obstacles with arbitrary l and w, but a fixed θ and (ii) Event $\mathcal{B}_i$: The reflection path at Z_i is not blocked by any other obstacles.

The event $\mathcal{A}_i$ occurs when the center of an obstacle resides on the $\overline{\mathrm{A}_i\mathrm{B}_i}$ (e.g., $\overline{\mathrm{A}_1\mathrm{B}_1}$ in Fig. 2(a)). The $L_{\overline{\mathrm{A}_i\mathrm{B}_i}}$ can be l or w, depending on which side of the obstacle tangent to the ellipse. However, because the area of a line is zero, the $\Pr_{\mathcal{A}_i}(\theta, r, D) = 0$. Instead, finding the PDF of $\mathcal{A}_i$ is of interest. To this end, we introduce the reflection points $\widehat{\mathrm{Z}}_i$, $i \in \{1, 2, 3, 4\}$ (e.g., $\widehat{\mathrm{Z}}_1$ in Fig. 2(a)) for the obstacles with the same orientation θ, but placed on ellipse $\Omega(r + dr)$ in Fig. 2(a), where dr is an infinitesimal increment of r. We denote the counterpart of $\overline{\mathrm{A}_i\mathrm{B}_i}$ for $\widehat{\mathrm{Z}}_i$ as $\overline{\widehat{\mathrm{A}}_i\widehat{\mathrm{B}}_i}$ (e.g., $\overline{\widehat{\mathrm{A}}_1\widehat{\mathrm{B}}_1}$). The region $\widehat{\mathrm{A}}_i\widehat{\mathrm{B}}_i\mathrm{B}_i\mathrm{A}_i$ is then a parallelogram that corresponds to the probability that obstacles with the fixed θ create

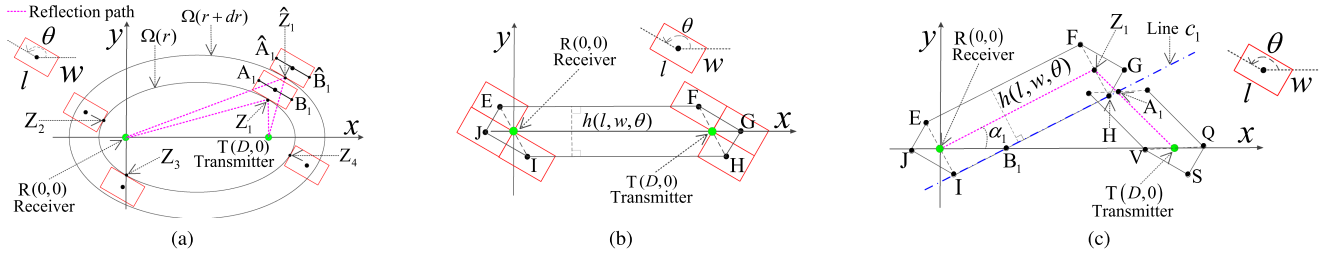

Fig. 2. MmWave P2P link $\overline{\mathrm{TR}}$ with length D: (a) Four possible reflection points on the ellipse $\Omega(r)$ in (4); (b) Region that the centers of obstacles with l, w, and θ falling in will block the $\overline{\mathrm{TR}}$; (c) Blockage of the first-order reflection path at Z_1.

reflection paths at the reflection points on $\overline{\mathrm{Z}_i\widehat{\mathrm{Z}}_i}$. One can first compute this probability. As the dr tends to 0, the PDF of $\mathcal{A}_i$ is attained by normalizing the probability by dr. This has previously been found in [7, (19)] as

$$f_{\mathcal{A}_i}(\theta, r, D) = \lambda_{Obs}\Upsilon_i r / \left(2\sqrt{r^2 - D^2\cos^2\theta}\right), \tag{5}$$

where $\Upsilon_i = E_l$ when $i = 1$ and 3 and $\Upsilon_i = E_w$ otherwise. The PDF of the first-order reflection path at Z_i is then obtained by

$$f_{\mathrm{Z}_i}(\theta, r, D) = f_{\mathcal{A}_i}(\theta, r, D)\mathrm{Pr}_{\mathcal{B}_i|\mathcal{A}_i}(\theta, r, D). \tag{6}$$

Provided (6), one can compute the average number of reflection paths of the P2P link $\overline{\mathrm{TR}}$ with length D as

$$E_N(D) = \sum_{i=1}^{4}\int_0^{\pi}\int_D^{R_{Max}} f_{\mathrm{Z}_i}(\theta, r, D)dr\, f_\theta(\theta)d\theta. \tag{7}$$

Finding $E_N(D)$ in (7) requires the expression for $\mathrm{Pr}_{\mathcal{B}_i|\mathcal{A}_i}(\theta, r, D)$ in (6). Although this has previously been studied in [1], [6], [10], their analytical models are tailored for circular obstacles [1], rectangular obstacles with common orientation [6], and line-shaped obstacles [10]. We will investigate, in Section IV, the model for the rectangular obstacles with random orientation in mmWave interference networks by exploiting the LoS blockage model in the below.

B. LoS Blockage Model

We introduce the LoS blockage model in [4] to compute the unblockage probability of an LoS link. According to [4, Theorem 1], the LoS path $\overline{\mathrm{TR}}$ in Fig. 2(b) is blocked when the center of an obstacle with l, w, and θ falls in the region EFGHIJ, where the area of EFGHIJ is given by $S_{\overline{\mathrm{TR}}}(l, w, \theta, D) = h(l, w, \theta)D + lw$. The $h(l, w, \theta)$ is the height of the parallelogram EFHI in Fig. 2(b) and the lw is the sum area of two right triangles EIJ and FGH in Fig. 2(b). The expectation of $S_{\overline{\mathrm{TR}}}(l, w, \theta, D)$ over l, w, and θ is then given by $E_{S_{\overline{\mathrm{TR}}}}(D) = E_h D + E_l E_w$, where $E_h = \frac{2(E_l + E_w)}{\pi}$. The number of the obstacles that block the $\overline{\mathrm{TR}}$ follows the Poisson distribution with mean $\lambda_{Obs}E_{S_{\overline{\mathrm{TR}}}}(D)$. Hence the unblockage probability of the path $\overline{\mathrm{TR}}$ is given by

$$\Pr_{\mathcal{C}}(D) = \exp\left(-\lambda_{Obs}E_{S_{\overline{\mathrm{TR}}}}(D)\right), \tag{8}$$

where $\mathcal{C}$ denotes the unblockage event of an LoS path.

IV. Reflection Path Blockage Analysis

We now derive an expression for the first-order reflection path blockage probability $\mathrm{Pr}_{\mathcal{B}_i|\mathcal{A}_i}(\theta, r, D)$ in (6), associated with the reflection point $\mathrm{Z}_i = \left(x_{\mathrm{Z}_i}(\theta, r, D), y_{\mathrm{Z}_i}(\theta, r, D)\right)$ in Fig. 2(a), in order to compute the $E_N(D)$ in (7). First, define $E_{S_{Ref_i}}(\theta, r, D)$ as the average area where the centers of obstacles falling in and those obstacles block the reflection path at Z_i. Then, the number of the obstacles blocking the reflection path is Poisson distributed with mean $\lambda_{Obs}E_{S_{Ref_i}}(\theta, r, D)$. If $E_{S_{Ref_i}}(\theta, r, D)$ is known, we have

$$\mathrm{Pr}_{\mathcal{B}_i|\mathcal{A}_i}(\theta, r, D) = \exp\left(-\lambda_{Obs}E_{S_{Ref_i}}(\theta, r, D)\right). \tag{9}$$

Hence, in what follows, we focus on finding the $E_{S_{Ref_1}}(\theta, r, D)$ associated with Z_1 in Fig. 2(a), keeping in mind that the exactly same analysis applies to compute the $E_{S_{Ref_i}}(\theta, r, D), i \in \{2, 3, 4\}$. For ease of notation, we will omit the (θ, r, D) from $E_{S_{Ref_1}}(\theta, r, D)$ in the sequel.

The reflection path at Z_1, which has two constituent line segments, i.e., $\overline{\mathrm{TZ}_1}$ and $\overline{\mathrm{RZ}_1}$, is illustrated in Fig. 2(c). The average area $E_{S_{\overline{\mathrm{RZ}_1}}}$ (resp., $E_{S_{\overline{\mathrm{TZ}_1}}}$) characterizing the blockage of $\overline{\mathrm{RZ}_1}$ (resp., $\overline{\mathrm{TZ}_1}$) follows the LoS blockage model in Fig. 2(b). There is non-negligible chance that an obstacle near Z_1 can simultaneously block the $\overline{\mathrm{TZ}_1}$ and $\overline{\mathrm{RZ}_1}$. Then simply adding $E_{S_{\overline{\mathrm{TZ}_1}}}$ and $E_{S_{\overline{\mathrm{RZ}_1}}}$ to obtain the $E_{S_{Ref_1}}$ is of low accuracy because of the overlap. On the other hand, analyzing the various cases of overlap events is prohibitively complicated. We overcome this difficulty by employing approximations.

A. Approximation of Average Area $E_{S_{Ref_1}}$

Similar to Fig. 2(b), the $\overline{\mathrm{RZ}_1}$ in Fig. 2(c) is blocked when the center of an obstacle with l, w, and θ falls in the EFGHIJ, whose average area is $E_{S_{\overline{\mathrm{RZ}_1}}} = E_h L_{\overline{\mathrm{RZ}_1}} + E_l E_w$. Similarly for $\overline{\mathrm{TZ}_1}$, we have $E_{S_{\overline{\mathrm{TZ}_1}}} = E_h L_{\overline{\mathrm{TZ}_1}} + E_l E_w$. We now approximate the $E_{S_{Ref_1}}$ by decoupling the correlation between the blockages of $\overline{\mathrm{TZ}_1}$ and $\overline{\mathrm{RZ}_1}$.

To this end, we first draw a Line c_1 in Fig. 2(c), which is obtained by extending $\overline{\mathrm{HI}}$. We then find a point A_1, the cross point between the Line c_1 and $\overline{\mathrm{TZ}_1}$. One can perceive that the blockages of $\overline{\mathrm{RZ}_1}$ and $\overline{\mathrm{A}_1\mathrm{Z}_1}$ are highly correlated, while the blockages of the $\overline{\mathrm{RZ}_1}$ and $\overline{\mathrm{TA}_1}$ are almost independent. Exploiting the high correlation between $\overline{\mathrm{RZ}_1}$ and $\overline{\mathrm{A}_1\mathrm{Z}_1}$ allows us to approximate the average area characterizing the blockage of the path constructed by $\overline{\mathrm{RZ}_1}$ and $\overline{\mathrm{A}_1\mathrm{Z}_1}$ as $E_{S_{\overline{\mathrm{RZ}_1}}}$. Then the near-independent blockage between $\overline{\mathrm{RZ}_1}$ and $\overline{\mathrm{TA}_1}$ leads to an approximation

$$E_{S_{Ref_1}} \approx E_{S_{\overline{\mathrm{RZ}_1}}} + E_{S_{\overline{\mathrm{TA}_1}}}, \tag{10}$$

where $E_{S_{\overline{\mathrm{TA_1}}}} \approx E_h L_{\overline{\mathrm{TA_1}}} + E_l E_w/2$, obtained by only including one right triangle VSQ in Fig. 2(c). This consideration is to reduce the overlap between $E_{S_{\overline{\mathrm{RZ_1}}}}$ and $E_{S_{\overline{\mathrm{TA_1}}}}$. We now look at the case when the Line c_1 has no cross point $\mathrm{A_1}$ with $\overline{\mathrm{TZ_1}}$. This happens when the Line c_1 is below the unintended transmitter T. This case represents highly correlated blockage between $\overline{\mathrm{RZ_1}}$ and $\overline{\mathrm{TZ_1}}$ and we have an approximation

$$E_{S_{Ref_1}} \approx E_{S_{\overline{\mathrm{RZ_1}}}}. \tag{11}$$

In summary, the approximation of $E_{S_{Ref_1}}$ is obtained by

$$E_{S_{Ref_1}} \approx \begin{cases} E_h\left(L_{\overline{\mathrm{RZ_1}}} + L_{\overline{\mathrm{TA_1}}}\right) + 3E_l E_w/2, & \text{if } \mathrm{A_1} \text{ exists} \\ E_h L_{\overline{\mathrm{RZ_1}}} + E_l E_w, & \text{otherwise} \end{cases}. \tag{12}$$

When computing the $L_{\overline{\mathrm{TA_1}}}$ in (12), the coordinates of $\mathrm{A_1}$ must be known. This can be done by finding the equation of Line c_1. Note that the $\overline{\mathrm{RZ_1}}$ and Line c_1 have the same slope $k_1 = y_{\mathrm{Z_1}}/x_{\mathrm{Z_1}}$ due to parallelism. As shown in Fig. 2(c), the intersection angle and the cross point between the Line c_1 and x-axis are $\alpha_1 = \arctan k_1$ and $\mathrm{B_1} = (x_{\mathrm{B_1}}, 0)$, respectively, where $x_{\mathrm{B_1}} = \frac{E_h}{2\sin\alpha_1}$. The equation of Line c_1 is therefore $y = k_1(x - x_{\mathrm{B_1}})$. Provided the equation of $\overline{\mathrm{TZ_1}}$, $y = \frac{y_{\mathrm{Z_1}}}{x_{\mathrm{Z_1}} - D}(x - D)$, the coordinates of $\mathrm{A_1}$ are given by the cross point between the $\overline{\mathrm{TZ_1}}$ and Line c_1.

When applying the above approach to the reflection paths at $\mathrm{Z}_i, i \in \{2,3,4\}$, we obtain, similar to (12), the $E_{S_{Ref_i}}$ s for $i \in \{2,3,4\}$. The $E_{S_{Ref_i}}$ s for $i \in \{1,2,3,4\}$ allow us to compute the $\Pr_{\mathcal{B}_i|\mathcal{A}_i}$ s using (9) and this leads to (6) and, consequently, (7). It should be mentioned that the average number of reflection paths $E_N(D)$ in (7) does not admit a closed-form expression, and hence it is calculated numerically.

V. Network Interference Analysis

In this section, we find the statistics of the number of interferers and derive the mean and CDF of the accumulated network interference power. These results are on the basis of the following independent blockage model.

A. Independent Blockage Model

When multiple links are close in location, one obstacle can simultaneously block some of them, implying that link blockage events are correlated in general. Nevertheless, in mmWave, ignoring the latter imposes less degradation on the accuracy of the analysis. This can be justified if there exist only a few interference paths without considering the blockage effect [4]. Unlike [4], where the independent blockage model was validated via simulation studies, we analytically verify the latter model based on the results in Section III-A in the below.

Denote the numbers of LoS and reflection interference paths without considering the blockage effect as Γ_{LoS} and Γ_{Ref}, respectively. We first focus on the Γ_{LoS}. Given the distance d of the intended LoS path, LoS interferers can only reside within the region outlined by $\mathbf{O}(d)$ and $\mathbf{O}(R_{Max})$. Since the average number of transmitters on a $\mathbf{O}(D), D \in [d, R_{Max}]$, is $2\pi D\lambda_{TX}$, the average total number of LoS interference paths without considering the blockage effect, for a given d, is given by

$$E_{\Gamma_{LoS}}(d) = \int_d^{R_{Max}} 2\pi D\lambda_{TX} \frac{\Delta_{TX}\Delta_{RX}}{4\pi^2} dD = \int_d^{R_{Max}} \xi D dD,$$

where $\xi \triangleq \lambda_{TX} \frac{\Delta_{TX}\Delta_{RX}}{2\pi}$. Taking the expectation of $E_{\Gamma_{LoS}}(d)$ with respect to the intended path distance d leads to

$$E_{\Gamma_{LoS}} = \int_0^{R_{Max}} \int_x^{R_{Max}} \xi D dD f_d(x) dx, \tag{13}$$

where $f_d(x)$ is in (1).

Denote by $E_M(D)$ the average number of the first-order reflection paths between an unintended transmitter on $\mathbf{O}(D)$ and the receiver without the blockage effect. Referring to the *Ellipse Model* in Section III-A, the $E_M(D)$ can be computed by changing the $f_{\mathrm{Z}_i}(\theta, r, D)$ in (7) to $f_{\mathcal{A}_i}(\theta, r, D)$ in (5), i.e.,

$$E_M(D) = \sum_{i=1}^{4} \int_0^{\pi} \int_D^{R_{Max}} f_{\mathcal{A}_i}(\theta, r, D) f_\theta(\theta)\, dr d\theta.$$

In our work, the reflection interferers are independent of d and can reside on any $\mathbf{O}(D)$ with $D \in (0, R_{Max}]$. Therefore, the total number of reflection interference paths is computed as

$$E_{\Gamma_{Ref}} = \int_0^{R_{Max}} \xi D E_M(D) dD. \tag{14}$$

The total average number of interference paths without considering the link blockage is then $E_{\Gamma_{Tot}} = E_{\Gamma_{LoS}} + E_{\Gamma_{Ref}}$ in (13) and (14). To evaluate the $E_{\Gamma_{Tot}}$, we set $l \in [10, 14]$ m, $w \in [5, 10]$ m, $\Delta_{TX} = 13$ degree, $\Delta_{RX} = 20$ degree, $\lambda_{TX} = 0.005$, and $\lambda_{Obs} \leq 0.0014$. Under this parameterization, there are on average 628 transmitters inside the $\mathbf{O}(R_{Max})$, $R_{Max} = 200$ m, and the $E_{\Gamma_{Tot}}$ is upper-bounded by $E_{\Gamma_{Tot}} \leq 3.8$. Compared to the simulation studies in [4] where the average number of interference paths guaranteeing the independent link blockage is found to be below 6, the $E_{\Gamma_{Tot}} \leq 3.8$ suffices to statistically ensure the independent blockage. Therefore, in the sequel, we focus on the network under the above parameterization and treat the blockage of individual link to be independent.

B. Statistics of Number of Interferers

In this subsection, we characterize the numbers of LoS and reflection interferers, denoted by K_{LoS} and K_{Ref}, respectively. The analysis is based on the derivations of $E_{\Gamma_{LoS}}$ in (13) and $E_{\Gamma_{Ref}}$ in (14), while considering the blockage effect.

With the above independent blockage model, the average number of LoS interferers on $\mathbf{O}(D)$ is given by $\upsilon_{LoS}(D) = \xi D \Pr_{\mathcal{C}}(D)$, where $\Pr_{\mathcal{C}}(D)$ is the LoS unblockage probability in (8). Referring to (13), the average number of LoS interferers in the network is obtained by

$$E_{K_{LoS}} = \int_0^{R_{Max}} \int_x^{R_{Max}} \upsilon_{LoS}(D) dD f_d(x) dx. \tag{15}$$

According to (15), the number $K_{LoS}(d)$ for a fixed $x = d$ follows a non-homogeneous Poisson distribution with the density $\upsilon_{LoS}(D), D \in [d, R_{Max}]$, and the mean $E_{K_{LoS}}(d) = \int_d^{R_{Max}} \upsilon_{LoS}(D) dD$, namely,

$$\Pr\left(K_{LoS}(d) = k\right) = e^{-E_{K_{LoS}}(d)} \left(E_{K_{LoS}}(d)\right)^k / k!.$$

Hence, the probability $\Pr(K_{LoS} = k)$, is computed as

$$\Pr(K_{LoS} = k) = \int_0^{R_{Max}} \Pr\left(K_{LoS}(x) = k\right) f_d(x) dx. \tag{16}$$

Similarly, from (14), the average number of reflection interferers on $\mathbf{O}(D)$ is given by $\upsilon_{Ref}(D)=\xi D E_N(D)$, where $E_N(D)$ is in (7). The average number of reflection interferers in the network is computed as

$$E_{K_{Ref}}=\int_0^{R_{Max}}\upsilon_{Ref}(D)dD. \tag{17}$$

Analogous to the above LoS case, the number of reflection interferers K_{Ref} in the network follows a non-homogeneous Poisson distribution with the density $\upsilon_{Ref}(D), D\in(0,R_{Max}]$, and the mean $E_{K_{Ref}}$. Thus,

$$\Pr\left(K_{Ref}=k\right)=e^{-E_{K_{Ref}}}\left(E_{K_{Ref}}\right)^k/k!.$$

Remark: A beam of an interferer may be aligned with the beam at the receiver through both the LoS and reflection paths or two reflection paths when: (i) The two paths exist and (ii) The two paths simultaneously reside in the mainlobe of the beams. In general, the joint probability of these two events is very low due to the path blockage, random reflection paths, and small Δ_{TX} and Δ_{RX}. Because the placements of interferers, obstacles, and beams are all i.i.d., we treat the LoS and reflection interferences are independent.

C. Mean of Accumulated Interference Power

The sum $q\in\{LoS,Ref\}$ interference can be written as

$$\Lambda_q=\sum_{i=1}^{K_q}I_q(r_i), \tag{18}$$

where $I_q(r_i)$ is the ith $q\in\{LoS,Ref\}$ interference power with the link length r_i and is computed by (3). Based on (18), the accumulated network interference power is given by

$$\Lambda_{Tot}=\Lambda_{LoS}+\Lambda_{Ref} \tag{19}$$

with the mean $E_{\Lambda_{Tot}}=E_{\Lambda_{LoS}}+E_{\Lambda_{Ref}}$. The E_{Λ_q} for $q\in\{LoS,Ref\}$ can be written as

$$E_{\Lambda_q}\overset{(a)}{=}E_{\left(K_q E_{I_q}\right)}=E_{K_q}E_{I_q}, \tag{20}$$

where (a) is due to the i.i.d. $\{I_q(r_i)\}$.

Calculating the E_{I_q} to find the E_{Λ_q} in (20) is of interest. From (15), for a fixed d, the PDF of an LoS interferer on $\mathbf{O}(D), D\in(d,R_{Max}]$, is obtained by $\upsilon_{LoS}(D)/E_{K_{LoS}}(d)$. Because all of the LoS interferers on $\mathbf{O}(D)$ have the same $I_{LoS}(D)$, we have

$$E_{I_{LoS}}=\int_0^{R_{Max}}\int_x^{R_{Max}}\frac{\upsilon_{LoS}(D)}{E_{K_{LoS}}(x)}I_{LoS}(D)\,dD f_d(x)dx. \tag{21}$$

Finding the $E_{I_{Ref}}$ requires a rather refined treatment. This is because, unlike the LoS interferers, the reflection interferers on $\mathbf{O}(D)$ can have different reflection path lengths $r(D)\in(D,D_{Max}]$, leading to different statistics of reflection interference power $I_{Ref}(r(D))$ for different $r(D)$ values. We first formulate the mean of $I_{Ref}(r(D))$ as

$$E_{I_{Ref}}(D)=\int_D^{R_{Max}}I_{Ref}(z)f_{r(D)}(z)dz, \tag{22}$$

where $f_{r(D)}(z)$ is the PDF of $r(D)$. With the $E_{I_{Ref}}(D)$ in (22), we obtain

$$E_{I_{Ref}}=\int_0^{R_{Max}}\frac{\upsilon_{Ref}(D)}{E_{K_{Ref}}}E_{I_{Ref}}(D)dD. \tag{23}$$

To find the $E_{I_{Ref}}$, the expression of $f_{r(D)}(z)$ in (22) is needed.

Because the reflection interferers on $\mathbf{O}(D)$ are i.i.d., we focus, without loss of generality, on a reflection interferer located at $(D,0)$. By the *Ellipse Model* in Section III-A, any point in the region outlined by the ellipse $\Omega(R_{Max})$ in (4) can be a reflection point of a reflection path between the reflection interferer at $(D,0)$ and the receiver. The area of the region is $\pi\frac{R_{Max}}{4}\sqrt{R_{Max}^2-D^2}$. The contribution of an ellipse $\Omega(z)$ to the latter area can be approximated as $\pi\frac{z+dz}{4}\sqrt{(z+dz)^2-D^2}-\pi\frac{z}{4}\sqrt{z^2-D^2}\overset{(b)}{\approx}\frac{\pi z}{2}dz-\frac{\pi D^2}{8z}dz$, where dz is an infinitesimal increment of z and (b) is due to the first-order Maclaurin series $x\sqrt{1-\frac{y^2}{x^2}}\approx x\left(1-\frac{y^2}{2x^2}\right)$. Hence we approximate the $f_{r(D)}(z)$ in (22) as

$$f_{r(D)}(z)\approx\frac{z/2-D^2/(8z)}{R_{Max}\sqrt{R_{Max}^2-D^2}/4}. \tag{24}$$

With the $f_{r(D)}(z)$ in (24), the $E_{I_{Ref}}$ in (23) is readily calculated.

Substituting (15), (17), (21), and (23) into (20) allows us to finally compute the $E_{\Lambda_{Tot}}=E_{\Lambda_{LoS}}+E_{\Lambda_{Ref}}$.

D. CDF of Accumulated Interference Power

The approach to find the CDF $\Pr(\Lambda_{Tot}\le x)$ is based on taking the Laplace transformation of Λ_{Tot},

$$\mathfrak{L}_{\Lambda_{Tot}}(s)=E_{e^{-s\Lambda_{LoS}}}E_{e^{-s\Lambda_{Ref}}}\overset{(c)}{=}\prod_{q\in\{LoS,Ref\}}E_{\left(E_{e^{-sI_q}}\right)^{K_q}}, \tag{25}$$

where (c) is due to the i.i.d. $\{I_q(r_i)\}$. The $E_{e^{-sI_{LoS}}}$ and $E_{e^{-sI_{Ref}}}$ in (25) are readily found by replacing the $I_{LoS}(D)$ in (21) with $e^{-sI_{LoS}(D)}$ and $I_{Ref}(z)$ in (22) with $e^{-sI_{Ref}(z)}$, respectively. With the $E_{e^{-sI_q}}$ for $q\in\{LoS,Ref\}$, we compute

$$E_{\left(E_{e^{-sI_q}}\right)^{K_q}}=\sum_{k=0}^{+\infty}\left(E_{e^{-sI_q}}\right)^k\Pr(K_q=k).$$

This allows us to find the $\mathfrak{L}_{\Lambda_{Tot}}(s)$ in (25).

The CDF $\Pr(\Lambda_{Tot}\le x)$ is now obtained by taking the inverse Laplace transformation of $\mathfrak{L}_{\Lambda_{Tot}}(s)/s$. However, analytically finding the inverse Laplace transform of $\mathfrak{L}_{\Lambda_{Tot}}(s)/s$ to have the closed-form expression of $\Pr(\Lambda_{Tot}\le x)$ is challenging. Instead, we exploit a numerical method, the Euler algorithm [11, (36)], to numerically compute the inverse Laplace transformation of $\mathfrak{L}_{\Lambda_{Tot}}(s)/s$. This operation is a standard numerical procedure and the details are omitted here.

VI. Numerical Results

We examine the proposed analytical interference models by comparing them with Monte-Carlo simulations. In the simulations, obstacles model buildings in urban scenarios with lengths $l\in[10,14]$ m and widths $w\in[5,10]$ m. We consider concrete buildings with the reflection loss $RL=7$ dB [9]. We set the $\Delta_{TX}=13$ degree and $\Delta_{RX}=20$ degree. The noise power in linear scale is given by $W_0=BW\cdot10^{-3+\frac{(ND+NF)}{10}}$ [12], where the bandwidth $BW=1$ GHz, thermal noise power density $ND=-174$ dBm/Hz, and noise figure $NF=9$ dB, resulting in $W_0=-105$ dB. Note that the same parameters were used to evaluate the $E_{\Gamma_{LoS}}$ in (13) and $E_{\Gamma_{Ref}}$ in (14).

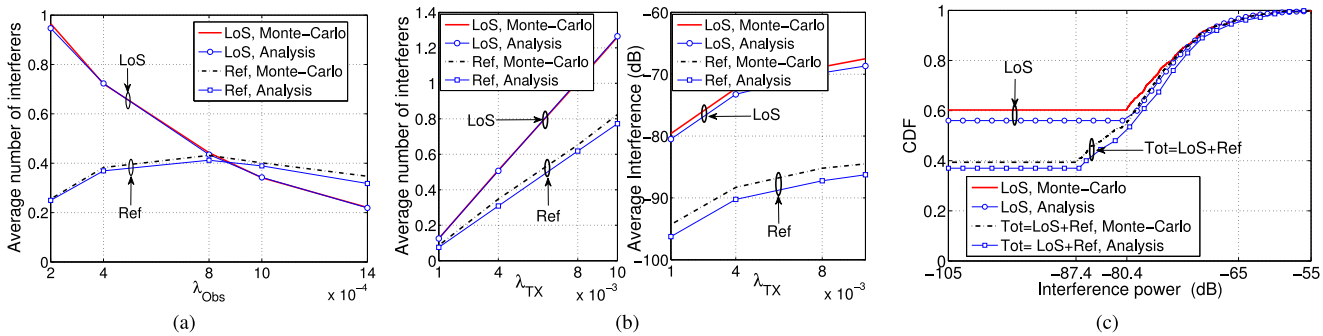

Fig. 3. (a) Average numbers of LoS and reflection interferers against λ_{Obs} for $\lambda_{TX}=0.005$; (b) Average numbers of LoS and reflection interferers and interference power across λ_{TX} for $\lambda_{Obs}=0.0005$; (c) CDFs of Λ_{LoS} and Λ_{Tot} in (19) when $\lambda_{TX}=0.005$ and $\lambda_{Obs}=0.0005$.

Fig. 3(a) shows the average numbers of LoS and reflection interferers $E_{K_{LoS}}$ in (15) and $E_{K_{Ref}}$ in (17), respectively, across λ_{Obs} for $\lambda_{TX}=0.005$. Tight matching between the analysis and Monte-Carlo simulations is evidenced. Seen from Fig. 3(a), the $E_{K_{LoS}}$ is monotonically decreasing with respect to λ_{Obs} due to the increased blockage. For reflection interferers, increasing λ_{Obs} generates more first-order reflection paths, but at the same time, increases the blockage. When $\lambda_{Obs}<0.0008$, the generation of reflection paths dominates the blockage of reflection paths, and thus the $E_{K_{Ref}}$ grows with λ_{Obs}. When $\lambda_{Obs}>0.0008$, opposite trend is observed since the blockage dominates the generation of reflection paths.

For fixed $\lambda_{Obs}=0.0005$, the E_{K_q} and E_{Λ_q} for $q\in\{LoS, Ref\}$ across λ_{TX} are displayed at the left and right subfigures of Fig. 3(b), respectively. Seen from the left subfigure, the $E_{K_{LoS}}$ and $E_{K_{Ref}}$ are linear with λ_{TX}, which is clear from (15) and (17). In the right subfigure, it can be seen that the $E_{\Lambda_{LoS}}$ is over 10 dB larger than the $E_{\Lambda_{Ref}}$. Since the $E_{K_{LoS}}$ and $E_{K_{Ref}}$ in the left subfigure are in the same order, the large gap between $E_{\Lambda_{LoS}}$ and $E_{\Lambda_{Ref}}$ is mainly due to the fact that the reflection pathloss is much higher than the LoS pathloss. Moreover, it is observed that both $E_{\Lambda_{LoS}}$ and $E_{\Lambda_{Ref}}$ are far larger than the noise power $W_0=-105$ dB.

Fig. 3(c) compares analytic CDF curves of the Λ_{Tot} and Λ_{LoS} in (19) with those of Monte-Carlo simulations when $\lambda_{TX}=0.005$ and $\lambda_{Obs}=0.0005$. Since $\Lambda_{Tot}\geq\Lambda_{LoS}$, when $\Lambda_{Tot}\leq x$, the Λ_{LoS} must satisfy $\Lambda_{LoS}\leq x$, yielding $\Pr(\Lambda_{Tot}\leq x)\leq\Pr(\Lambda_{LoS}\leq x)$. The minimum Λ_q (i.e., $\Lambda_q=I_q(R_{Max})$ in (3)) for $q\in\{LoS, Ref\}$ are -80.4 dB and -87.4 dB, respectively. This reveals, in Fig. 3(c), the constant CDF $\Pr(\Lambda_{Tot}\leq x)$ for $x\in[-105,-87.4]$ (resp., $\Pr(\Lambda_{LoS}\leq x)$ for $x\in[-105,-80.4]$) dB. About 0.2 CDF difference between $\Pr(\Lambda_{LoS}\leq x)$ and $\Pr(\Lambda_{Tot}\leq x)$ at $x\in[-105,-87.4]$ dB and the drastic increase of the CDF of Λ_{Tot} at $x\in(-87.4,-80.4]$ dB demonstrate the impact of the reflection interference in the network. When $x\in[-80.4,-55]$ dB, we find $\Pr(\Lambda_{LoS}\leq x)\approx\Pr(\Lambda_{Tot}\leq x)$. This is because the Λ_{Ref} is much smaller than the Λ_{LoS}, as seen from Fig. 3(b). When the LoS and reflection interferences coexist, the LoS interference overwhelms the reflection counterpart.

VII. Conclusion

We proposed analytical interference models characterizing the accumulated interference power in a dense urban mmWave network in the presence of geometry-dependent first-order reflection paths. The statistics of the numbers of LoS and reflection interferers and the mean and CDF of the accumulated network interference power were derived. Simulation results demonstrated the accuracy of the analysis and showed that the dense mmWave network is often interference-limited. The geometry-dependent reflection interference is non-negligible. It is indeed an indispensable component in characterizing the mmWave network.

References

[1] H. Shokri-Ghadikolaei and C. Fischione, "The transitional behavior of interference in millimeter wave networks and its impact on medium access control," *IEEE Trans. Commun.*, vol. 64, no. 2, pp. 723–740, Feb. 2016.

[2] V. Petrov, M. Komarov, D. Moltchanov, J. M. Jornet, and Y. Koucheryavy, "Interference and SINR in millimeter wave and terahertz communication systems with blocking and directional antennas," *IEEE Trans. Wireless Commun.*, vol. 16, no. 3, pp. 1791–1808, Mar. 2017.

[3] S. Singh, M. N. Kulkarni, A. Ghosh, and J. G. Andrews, "Tractable model for rate in self-backhauled millimeter wave cellular networks," *IEEE J. Sel. Areas Commun.*, vol. 33, no. 10, pp. 2196–2211, Oct. 2015.

[4] T. Bai, R. Vaze, and R. W. Heath, "Analysis of blockage effects on urban cellular networks," *IEEE Trans. Wireless Commun.*, vol. 13, no. 9, pp. 5070–5083, Sep. 2014.

[5] T. S. Rappaport and S. Deng, "73 GHz wideband millimeter-wave foliage and ground reflection measurements and models," in *Proc. IEEE Int. Conf. Commun. Workshop*, Jun. 2015, pp. 1238–1243.

[6] N. A. Muhammad, P. Wang, Y. Li, and B. Vucetic, "Analytical model for outdoor millimeter wave channels using geometry-based stochastic approach," *IEEE Trans. Veh. Technol.*, vol. 66, no. 2, pp. 912–926, Feb. 2017.

[7] T. S. Rappaport *et al.*, "Millimeter wave mobile communications for 5G cellular: It will work!" *IEEE Access*, vol. 1, pp. 335–349, 2013.

[8] M. R. Akdeniz, Y. Liu, M. K. Samimi, S. Sun, S. Rangan, and T. S. Rappaport, "Millimeter wave channel modeling and cellular capacity evaluation," *IEEE J. Sel. Areas Commun.*, vol. 32, no. 6, pp. 1164–1179, Jun. 2014.

[9] S. Larew, T. Thomas, M. Cudak, and A. Ghosh, "Air interface design and ray tracing study for 5G millimeter wave communications," in *Proc. IEEE Globecom Workshops*, Dec. 2013, pp. 117–122.

[10] A. K. Gupta, J. G. Andrews, and R. W. Heath, "Macro diversity in cellular networks with random blockages," *IEEE Trans. Wireless Commun.*, vol. 17, no. 2, pp. 996–1010, Feb. 2018.

[11] J. Abate and W. Whitt, "A unified framework for numerically inverting laplace transforms," *INFORMS J. Comput.*, vol. 18, no. 4, pp. 408–421, Jan. 2006.

[12] M. Rupp, S. Schwarz, and M. Taranetz, *The Vienna LTE-Advanced Simulators: Up and Downlink, Link and System Level Simulation* (Signals and Communication Technology), 1st ed. Singapore, Springer, 2016.